




Cite this: *RSC Adv.*, 2025, 15, 32143

Metal–organic framework–injectable hydrogel hybrid scaffolds promote accelerated angiogenesis for *in vivo* tissue engineering

Sobuj Shahidul Islam, Tatsuya Dode, Soma Kawashima, Myu Fukuoka, Takaaki Tsuruoka * and Koji Nagahama *

The application of nanoscale metal–organic frameworks (MOFs) in tissue engineering is receiving increased attention. As three-dimensional scaffolding materials that provide an appropriate extracellular microenvironment supporting the survival, proliferation, and organization of cells play a key role *in vivo* tissue engineering, hybridization of nanoscale MOFs with bulk hydrogels has led to the development of nanoscale MOF–combined hydrogels. However, development of nanoscale MOF–combined hydrogel scaffolds remains challenging. Generally, since the gelation properties of injectable hydrogels are delicate, the sol–gel transition behavior could be lost due to the influence of additives. To date, little progress has been made in the development of nanoscale MOF–combined injectable hydrogel scaffolds. Herein, we propose a novel injectable hydrogel scaffold generated by combining NU-1000 nanoscale MOFs with PLGA-PEG-PLGA/LAPONITE® nanocomposite hydrogels. The resultant PLGA-PEG-PLGA/LAPONITE®/L-Arg@NU-1000 hybrid hydrogels exhibited sustained slow release of L-arginine over 1 month. The precursor solution of PLGA-PEG-PLGA/LAPONITE®/L-Arg@NU-1000 undergoes rapid sol–gel transition upon exposure to body temperature, enabling focal administration of the hydrogel at desired locations in the body *via* simple injection. The sustained L-arginine–slow release capability of the hybrid hydrogels results from the functionality of NU-1000 as a primary carrier and efficiently facilitates angiogenesis *in vivo*. The hybrid hydrogel exhibits highly specific functionality as a scaffold that cannot be achieved using NU-1000 alone or PLGA-PEG-PLGA/LAPONITE® hydrogels alone, thus indicating that the hybrid injectable hydrogels have the potential to become a new type of scaffold for tissue engineering.

Received 21st April 2025
Accepted 11th August 2025

DOI: 10.1039/d5ra02770e

rsc.li/rsc-advances

Introduction

Metal–organic frameworks (MOFs) are organic–inorganic hybrid porous materials. Compared with conventional organic and inorganic materials, MOFs offer the advantages of compositional and structural diversity, high porosity, ultrahigh specific surface area, and excellent thermal and chemical stability.^{1–3} Due to their unique structure and properties, MOFs are used in a wide variety of applications, including gas storage,^{4,5} catalysis,^{6,7} and sensing.^{8,9} Over the last decade, an increasing number of studies have focused on the application of nanoscale MOFs for biomedical purposes. Due to their high surface area and excellent porosity, nanoscale MOFs are ideally suited for use as nanocarriers in drug delivery systems, enabling long-term, controlled release of small-molecule drugs.^{10–12} Recently, the application of nanoscale MOFs in tissue engineering has also been receiving increased attention.^{13–18} As three-dimensional scaffolding materials that provide an

appropriate extracellular microenvironment supporting the survival, proliferation, and organization of cells play a key role *in vivo* tissue engineering, several studies have attempted the hybridization of nanoscale MOFs with bulk materials such as fibers, sponges, and needles.^{19–22} Hydrogels are well-suited for use as three-dimensional scaffolding materials in tissue engineering due to their biocompatibility, high water content, and softness, and several studies have reported the development of nanoscale MOF–hydrogel hybrids.^{23–27} Yin *et al.* introduced Mg-based MOFs into a poly(γ -glutamic acid) hydrogel which was then loaded in a microneedle patch. This MOF–hybrid gel promoted angiogenesis by slowly releasing Mg²⁺. The results of *in vivo* experiments showed that the addition of these MOFs increased the capillary density around wounds, indicating that this treatment increases the rate of neovascularization.²⁶ Wang *et al.* reported that an miR-29a-loaded ZIF-8 encapsulated silk fibroin/gelatin hydrogel conduit promoted the myelination of Schwann cells and the neuronal differentiation and axonal elongation of PC12 cells. Their study not only demonstrated the potential application of ZIF-8 as nanocarrier for miR-29a in peripheral nerve repair but also highlighted the potential usefulness of ZIF-8 in peripheral nerve repair.²⁷ As nanoscale

Department of Nanobiochemistry, Frontiers of Innovative Research in Science and Technology (FIRST), Konan University, 7-1-20 Minatojima-minamimachi, Chuo-ku, Kobe 650-0047, Japan. E-mail: nagahama@konan-u.ac.jp; tsuruoka@konan-u.ac.jp



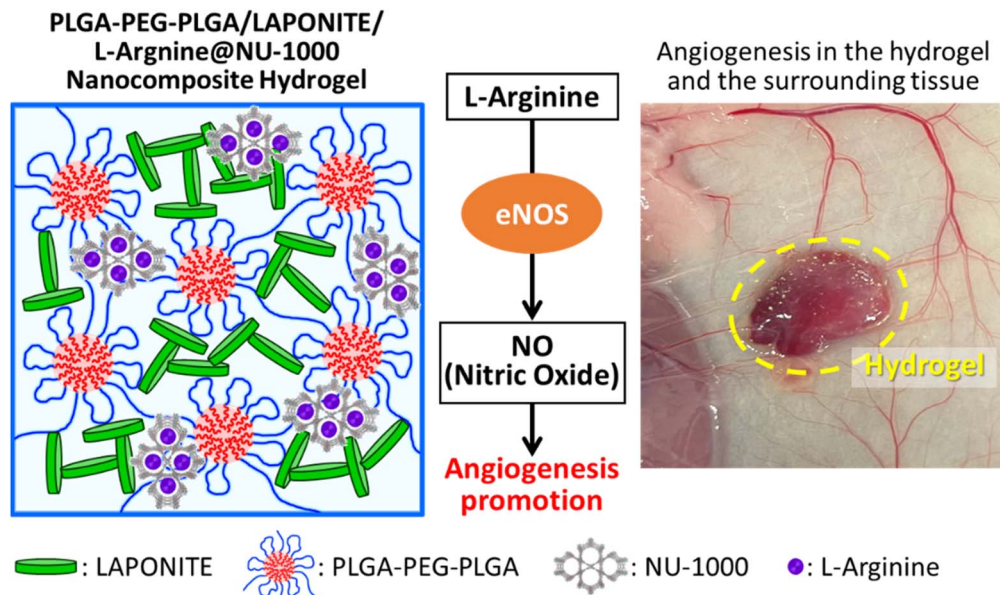


Fig. 1 Illustration of the network structure of PLGA-PEG-PLGA/LAPONITE@/L-Arg@NU-1000 hybrid injectable hydrogels and example of angiogenesis promotion.

MOF-hydrogel hybrid scaffolds exhibit high functionality that cannot be achieved using nanoscale MOFs alone or hydrogels alone, nanoscale MOF-hydrogel hybrids could represent a new, highly useful type of scaffolding material in tissue engineering. However, the development of nanoscale MOF-hydrogel hybrid scaffolds remains challenging. Generally, since the gelation properties of injectable hydrogels are delicate, the sol-gel transition behavior could be lost due to the influence of additives. To date, little progress has been made in the development of nanoscale MOF-combined injectable hydrogel scaffolds. Injectable hydrogels represent one of the most promising types of scaffolding materials for *in vivo* tissue engineering, and intensive studies over the past several decades have led to the development of a variety of injectable hydrogels. Injectable hydrogels are preferable for clinical use, as they exhibit sol-gel transition after injection into the body. Because solutions of injectable hydrogel precursors can readily entrap various bioactive matrices, such as cells and drugs, these solutions can be injected to form a hydrogel that entraps bioactive matrices. This allows the construction of a regenerative environment *in situ* through a minimally invasive implantation procedure.^{28–30} Based on this background, we developed the first example of a nanoscale MOF-injectable hydrogel hybrid scaffold and investigated its potential utility *in vivo* tissue engineering.

We recently developed an injectable hydrogel generated by hierarchical self-assembly of disk-shaped clay nanoparticles (LAPONITE®) and biodegradable poly(DL-lactide-co-glycolide)-*b*-poly(ethylene glycol)-*b*-poly(DL-lactide-co-glycolide) copolymers (PLGA-PEG-PLGA) (Fig. S1, SI).^{31–33} The precursor solution of PLGA-PEG-PLGA/LAPONITE® was shown to rapidly undergo sol-gel transition upon exposure to body temperature, thus enabling focal hydrogel administration at desired locations in the body *via* simple injection. For the present study, we selected

NU-1000, which are stable against water and body temperature, biocompatible, zirconium-based nanoscale MOFs.^{34,35} The structure of NU-1000 MOFs includes hexa-Zr nodes ($[\text{Zr}_6\text{O}_4(\text{OH})_4]^{8+}$) connected *via* a tetra topic linker (1,3,6,8-tetrakis [*p*-benzoic acid] pyrene, H_4TBAPy). The mature structure contains 3 nm hexagonal pores with inward-facing hydroxyl groups. Moreover, NU-1000 was selected as the MOF because of its high biocompatibility and high stability in water at body temperature, as well as its porous size match with the size of L-arginine.³⁶ L-Arginine was selected as a bioactive molecule in this study. The angiogenic effects of L-arginine reportedly involve the restoration of defective NO synthesis and pathways, thus increasing NO bioavailability.^{37,38} In tissue engineering, neovascularization is essential for proper regeneration and functional recovery of injured tissues. In this study, we first prepared L-arginine-loaded NU-1000 (L-arginine@NU-1000), which was then combined with PLGA-PEG-PLGA/LAPONITE® composites to give PLGA-PEG-PLGA/LAPONITE®/L-arginine@NU-1000 hybrids (Fig. 1). We previously reported the successful regeneration of skeletal muscle tissue using PLGA-PEG-PLGA/LAPONITE®/L-arginine@NU-1000 hybrid injectable gel potential by angiogenesis promotion.³⁹ However, the details of the angiogenesis-promoting effect of the gel have not yet been investigated. Therefore, in this study, we attempt to clarify the angiogenic effects of the hydrogels. Moreover, we evaluated the effects of the concentrations of polymer and LAPONITE® on the angiogenic effects in this study. To this end, the potential utility of PLGA-PEG-PLGA/LAPONITE®/L-arginine@NU-1000 hybrid injectable hydrogels for *in vivo* tissue engineering applications was assessed by investigating their physicochemical and L-arginine-release properties, biodegradation, *in vitro* cell compatibility, and *in vivo* angiogenic activity.



Materials and methods

Materials

Poly(ethylene glycol) (PEG; MW: 3.0 kDa), glycolide (GA), and tin-2-ethyl hexanoate were purchased from Sigma-Aldrich Japan (Tokyo, Japan). L-Lactide (L-LA) and D-lactide (D-LA) were purchased from Musashino Chemical Laboratory Ltd (Tokyo, Japan) and purified by lyophilization. LAPONITE® was kindly supplied by Wilbur-Ellis Co., Ltd (Tokyo, Japan). L-Arginine and ninhydrin were purchased from Fujifilm Wako Pure Chemical Co., Ltd (Osaka, Japan). Zirconium chloride and sodium hydroxide were purchased from Fujifilm Wako Pure Chemical Co. 4,4',4'',4'''-(pyrene-1,3,6,8-tetrayl) tetra benzoic acid (H4TBAPy), and N,N-dimethylformamide (DMF) were purchased from Sigma-Aldrich. 4-Biphenylcarboxylic acid was purchased from Tokyo Chemical Industry Co., Ltd. We have also used the other materials received for further purification.

Preparation of NU-1000

The ZrCl_4 (69.2 mg, 0.279 mmol) and 4-biphenylcarboxylic acid (3.16 g, 15.9 mmol) were dissolved in DMF (8 mL) with sonication before heating at 80 °C for 1 hour using an aluminum heating block. Meanwhile, H4TBAPy (50.3 mg, 73.7 μmol) was dissolved in DMF (3 mL) with sonication before addition of 1 M NaOH aqueous solution (36 μL). After mixing the Zr-based and H4TBAPy solutions, the resulting mixture was heated at 100 °C for 24 hours. After heating, the resulting samples were filtrated using 0.2 μm membrane filter, washed with DMF three times, and dried at 120 °C under the vacuum to give slight yellow powder of NU-1000.

Preparation of L-arginine NU-1000

One mg of NU-1000 was taken into a glass vial and 1 mL of L-arginine/Milli-Q water solution (1.5 mg mL^{-1}) was added to the vial, then the suspension was stirred (200 rpm) at 37 °C for the appropriate time (1 to 10 days). The resulting samples were washed with Milli-Q water three times and dried under the vacuum to give slight yellow powder of L-arginine-loading NU-1000. For standard preparation, L-arginine with different amounts was taken into a microtube, then 1 mL Milli-Q water was added to dissolve it, and 1 mL of 4% ninhydrin solution was added. After that, took this sample for 3 hours in a dark place and measured this sample by a UV-vis spectroscopic analyzer.

Preparation and characterization of L-arginine@NU-1000/PLGA-PEG-PLGA/LAPONITE® hybrid hydrogels

PLGA-PEG-PLGA was synthesized *via* bulk ring-opening copolymerization of L-LA, D-LA, and GA in the presence of PEG using tin 2-ethylhexanoate as a catalyst. Briefly, under a nitrogen atmosphere, PEG (2250 mg, 0.75 mmol), L-LA (972 mg, 6.75 mmol), D-LA (972 mg, 6.75 mmol), GA (783 mg, 6.75 mmol), and tin 2-ethylhexanoate (12 mg, 30 μmol) were mixed in a glass flask and dried under vacuum overnight. The flask was then purged with nitrogen and sealed tightly. The sealed flask was placed in an oil bath at 150 °C for 6 hours. The reaction mixture

was dissolved in chloroform and dropped into an excess amount of diethyl ether, and the resultant precipitate was then dried under vacuum overnight to give PLGA-PEG-PLGA. The M_n and M_w/M_n of the synthesized copolymers were determined by gel permeation chromatography (GPC) (JASCO, HPLC LC-2000Plus; column, TSK gel; detectors, RI and UV; standard, PEG; eluent, 10 mM LiBr in DMSO). The molecular compositions of PEG, LA, and GA in the copolymers were estimated from ^1H -nuclear magnetic resonance (NMR) measurements (JEOL, ECA-500, solvent: CDCl_3). 100 mg of PLGA-PEG-PLGA copolymer was dissolved in 1 mL of acetone, and then 1 mL of pure water was added to the solution. The mixture was gently stirred, and acetone was gradually evaporated *via* aspiration to prepare aqueous solution of PLGA-PEG-PLGA (10%). Specific amount of L-arginine-loading NU-1000 was dispersed in 10% PLGA-PEG-PLGA solution (1 mL), then 1 mL of LAPONITE® aqueous solution (1.8, 2.2, 2.6%) was added to each PLGA-PEG-PLGA (10%)/L-arginine@NU-1000 dispersion and vigorously stirred to prepare PLGA-PEG-PLGA (5%)/LAPONITE® (0.9, 1.1, 1.3%)/L-arginine@NU-1000 nanocomposites. Rheological analysis of the PLGA-PEG-PLGA (5%)/LAPONITE® (0.9, 1.1, 1.3%)/L-arginine@NU-1000 nanocomposites were performed. The nanocomposites with sol state were incubated at 4 °C for 10 min, and then their temperature-responsive sol-gel transition was investigated by rheometer (MCR302, Anton Paar). To visualize the gel networks, the nanocomposite gels, PLGA-PEG-PLGA (5%)/LAPONITE® (0.9%) and PLGA-PEG-PLGA (5%)/LAPONITE® (0.9%)/L-arginine@NU-1000, were lyophilized and stained with osmium, were analyzed by scanning electron microscopy (SEM) (JSM-7001FA, JEOL). The pore size of the gels was analyzed by using the SEM images and the values were represented as mean \pm SD ($N = 15$).

L-Arginine controlled release properties of the hybrid hydrogels

For standard preparation, L-arginine with different amounts was taken into a microtube, then 1 mL PBS was added to dissolve it, and 1 mL of 4% ninhydrin solution was added. After that, took this sample for 3 hours in a dark place and measured this sample by a UV-vis spectroscopic analyzer. PLGA-PEG-PLGA (5%)/LAPONITE® (0.9, 1.1, 1.3%)/L-arginine@NU-1000 nanocomposite hydrogels (330 μL) were prepared in the multiple well plate, and then 1000 μL of PBS (pH 7.4) were added into the well and incubated at 37 °C for appropriate time. Afterward, 500 μL of supernatant was collected at predetermined time intervals and added 500 μL of fresh PBS. 500 μL of 4% ninhydrin solution was added into the collected supernatant samples and place at the dark place for 3 hours to give reactions between L-arginine with ninhydrin. Finally, the resultant sample was treated by 0.22 μm filtration, and then the amount of L-arginine was quantified by UV-spectroscopy measurements at 400 nm.

Cytocompatibility of the hybrid hydrogels

PLGA-PEG-PLGA (5%)/LAPONITE® (0.9, 1.1, 1.3%)/L-arginine@NU-1000 nanocomposite hydrogels (330 μL) were prepared in the insert of Transwell. After that, HUVEC cells (2.0



$\times 10^4$) were cultured into the 24 well plate in the presence of the nanocomposite hydrogels for 1, 3, and 7 days. After that cells were washed with HEPES buffer twice carefully and live/dead assay using calcine-AM and PI was performed and the images were obtained by fluorescence microscopy (BZ-9000, KEYENCE). The number of cells per field and cell viability was quantified using the images.

Biodegradation of the hybrid hydrogels

PLGA-PEG-PLGA (5%)/LAPONITE® (0.9, 1.1, 1.3%)/L-arginine@NU-1000 nanocomposite hydrogels (300 μ L) were prepared in microtube, and then 700 μ L of PBS (pH 7.4) was added onto the gels and incubated at 37 °C. After 5, 10, 15, and 20 days, the supernatant was completely removed, and the gels were dried by lyophilization. The dried gels were weighted and degradation ratio were quantified.

Swelling ratio of the hybrid hydrogels

Injectable hydrogels including P5L0.9, P5L0.9/L-Arg@NU-1000, P5L1.1, P5L1.1/L-Arg@NU-1000, P5L1.3, and P5L1.3/L-Arg@NU-1000 were prepared. Approximately 150 μ L of each hydrogel was transferred into pre-weighed 1 mL Eppendorf tubes. The net initial weight of each hydrogel sample was recorded by subtracting the weight of the empty tube. The samples were incubated at 37 °C with 5% CO₂ for 30 minutes to equilibrate under physiological conditions. Subsequently, 600 μ L of (1 \times PBS) was carefully added to each tube to initiate the swelling process. At pre-determined time intervals (1 to 12 hours), the PBS was gently removed, and the swollen hydrogels were weighed again to determine the mass increase due to water uptake. The swelling ratio was calculated based on the weight difference before and after swelling. All measurements were performed in triplicate, and results are reported as mean \pm SD. Swelling ratio = W_t/W_o . W_t = weight of the swelled gels and W_o = Initial weight of the gels.

Hemolysis test of hybrid hydrogels

Injectable hydrogel formulations including P5L0.9, P5L0.9/L-Arg@NU-1000, P5L1.1, P5L1.1/L-Arg@NU-1000, P5L1.3, and P5L1.3/L-Arg@NU-1000 were prepared. For each sample, approximately 200 μ L of hydrogel was transferred into pre-weighed 2 mL Eppendorf tubes. The samples were then incubated at (37 °C with 5% CO₂) for 30 minutes to simulate physiological conditions. Following incubation, 1 μ L of (1 \times PBS) was gently added on top of each hydrogel. After 5 days of incubation, the overlying PBS was carefully collected and transferred to fresh 1 mL Eppendorf tubes for hemolysis testing. Whole blood was collected from healthy nude mice and anticoagulated by mixing with 1 M sodium citrate at a 9 : 1 (v/v) ratio. The anti-coagulated blood was centrifuged at 1000 \times g for 5 minutes to separate the red blood cells (RBCs), which were then washed twice with (1 \times PBS) to remove plasma components. For hemolysis evaluation, the washed RBCs were mixed with the collected PBS extracts from the hydrogels. Controls were prepared using (1 \times PBS) (negative control) and Milli-Q water (positive control). All mixtures were incubated at 37 °C for 1

hour, followed by centrifugation at 1000 \times g for 5 minutes. Subsequently, 500 μ L of the supernatant from each sample was collected, and the absorbance at 545 nm was measured using a UV-vis spectrophotometer to determine the release of hemoglobin. The percentage of hemolysis was calculated based on the absorbance values of the test samples in comparison with the positive and negative controls. All experiments were performed in triplicate, and data were expressed as mean \pm SD. Hemolysis rate (%) = (sample) – (negative control)/(positive control) – (negative control).

Angiogenic capability of the hybrid hydrogels

All animal experiments and all experimental protocols were approved by Konan University (K-23-05) and conformed to the Guidelines for the Care and Use of Laboratory Animals published by the National Institutes of Health. Mice (ICR CrI/CD1, 4 weeks old, female) were anesthetized with isoflurane. Five hundred microliters of PLGA-PEG-PLGA (5%)/LAPONITE® (0.9, 1.1, 1.3%)/L-arginine@NU-1000 nanocomposite hydrogels were injected subcutaneously into the muscle layer of the back using a syringe with a 24-gauge needle. After 7, 14, and 21 days, the degree of vascularization was quantified using the scoring as follows.⁴⁰ Angiogenesis scoring; BMS (Biomaterial Score): The degree of vascularization (e.g., redness, blood vessels) within and/or around the edge of the biomaterial. 0: no blood vessel perfusion within biomaterial, 2: slightly red within biomaterial or at the periphery, 4: biomaterials appear very red in color with evidence of some blood vessels sprouting, 6: significant blood vessel perfusion: biomaterial is totally red or dark red, with lots of mature vessels growing within. We have performed the three different experiments in triplicate and data were expressed as mean \pm SD.

Histological analysis of the hybrid hydrogels

Mice (ICR CrI/CD1, 4 weeks old, female) were anesthetized with isoflurane. Five hundred microliters of PLGA-PEG-PLGA (5%)/LAPONITE® (0.9, 1.1, 1.3%)/L-arginine@NU-1000 nanocomposite hydrogels were injected subcutaneously into the muscle layer of the back using a syringe with a 24-gauge needle. After 7, 14, and 21 days, the mice were sacrificed and the hydrogels and the surrounding tissues were carefully excised, cryosections of the samples were prepared (Thermo Scientific, CryoStar NX70). The cryosections were immunostained with Alexa Fluor®567-labeled anti-CD31 antibody, then analyzed by fluorescence microscopy (BZ-9000, KEYENCE). The number of blood vessels per field and their diameter newly formed in the nanocomposite hydrogels were quantified using the corresponding images. We have performed the three different experiments in triplicate and data were expressed as mean \pm SD.

Results and discussion

Characterizations of L-arginine-loaded NU-1000/PLGA-PEG-PLGA/LAPONITE® hybrid hydrogels

NU-1000 was prepared as reported previously,³⁴ and the formation of crystalline NU-1000 was confirmed by scanning



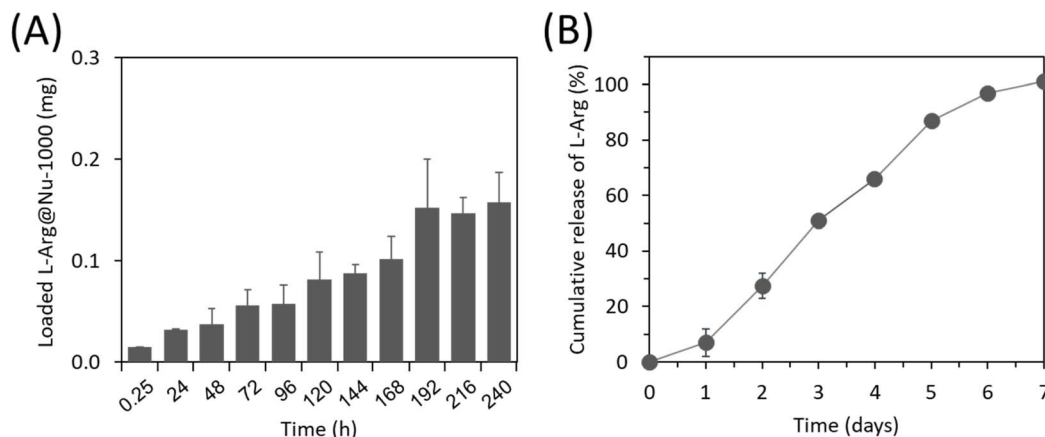


Fig. 2 (A) The amounts of L-arginine loaded in 1.0 mg of NU-1000 and (B) profile of cumulative L-arginine release from NU-1000.

electron microscopy (SEM) (Fig. S2, SI) and X-ray diffraction analyses (Fig. S3, SI). Aqueous solutions of L-arginine were mixed vigorously with NU-1000 for a predetermined time and then centrifuged. The supernatant containing unloaded L-arginine was reacted with ninhydrin, and the absorbance of the reactants was determined using UV-vis spectroscopy to determine the amount of L-arginine not loaded to the NU-1000 hydrogels. Based on these values and the feeding amount of L-arginine (1.5 mg), the amount of L-arginine loaded to 1 mg of NU-1000 was quantified (Fig. 2A). The amount of loaded L-arginine increased over time and reached an equilibrium after 192 hours, indicating that L-arginine-loaded NU-1000 (L-Arg@NU-1000) and NU-1000 act as primary carriers for L-arginine. Analysis of the quantity of L-arginine loaded to NU-1000 indicated that maximum loading occurred after 192 hours, with 152 μ g of L-arginine loaded to 1 mg of NU-1000. To exploit the biological activity of L-arginine and accelerate neo-vascularization, sustained slow release of L-arginine is essential. We therefore investigated the kinetics of L-arginine release from NU-1000. These analyses revealed that NU-1000 provides sustained slow release of L-arginine for 7 days until reaching 100%, without an initial burst release (Fig. 2B).

PLGA-PEG-PLGA copolymer was synthesized *via* anionic ring-opening polymerization of L-LA, D-LA, and GA in the presence of PEG as a macroinitiator (Scheme S1, SI). The molecular composition, molecular weight, and molecular weight distribution were determined by $^1\text{H-NMR}$ spectroscopy in CDCl_3 and GPC analysis. The resulting PLGA-PEG-PLGA exhibited a unimodal GPC curve with a molecular weight distribution of less than 1.3. These data are summarized in (Table S1, SI). PLGA-PEG-PLGA/LAPONITE® composite hydrogels of varying composite ratios were prepared by simple mixing of aqueous solutions of PLGA-PEG-PLGA and LAPONITE® at specific concentrations. The PLGA-PEG-PLGA/LAPONITE® hydrogels examined in this study are indicated herein according to the concentrations of PLGA-PEG-PLGA and LAPONITE®. For instance, the designation P5L0.9 refers to a hydrogel consisting of 5.0% PLGA-PEG-PLGA and 0.9% LAPONITE®. The present

study evaluated P5L0.9, P5L1.1, and P5L1.3 hydrogels in terms of hybridization with L-arginine@NU-1000.

We previously reported construction of the network structure of PLGA-PEG-PLGA/LAPONITE® composite hydrogels *via* hierarchical self-assembly of PLGA-PEG-PLGA nanomicelles and LAPONITE® nanoparticles.⁴¹ Briefly, hydrogen bonds form the main interactions of the physical cross-linking points between the hydroxyl groups of LAPONITE® located on the planar surface and ether oxygen molecules of the PEG segments in the nanomicelles. Notably, although the PLGA-PEG-PLGA nanomicelle solution exhibited reversible thermo-gelation, the PLGA-PEG-PLGA/LAPONITE® composite solution underwent irreversible thermo-gelation due to physical cross-linking through the interactions between LAPONITE® and PLGA-PEG-PLGA nanomicelles. Similarly, NU-1000 possesses surface carboxyl residues associated with the tetracarboxylate ligand H4TBAPy that can form hydrogen bonds with the hydroxyl groups of LAPONITE®.³⁹ Considering that NU-1000 can thus interact with LAPONITE®, we hypothesized that the gelation behavior of PLGA-PEG-PLGA/LAPONITE® composite hydrogels can be modulated in the presence of L-Arg@NU-1000. We therefore investigated the effect of L-Arg@NU-1000 on the thermo-responsive sol-gel transition behavior of PLGA-PEG-PLGA/LAPONITE® hydrogels. P5L0.9, P5L1.1, and P5L1.3 composites exhibited thermo-gelation in the presence of L-Arg@NU-1000, and slightly turbid hydrogels were formed at 37 °C (Fig. 3A). shows photographs of P5L1.1 composites in the presence of L-Arg@NU-1000 in the sol state at room temperature and gel state at 37 °C. The thermo-gelation was completely irreversible; the generated P5L1.1/L-Arg@NU-1000 hybrid hydrogels did not transition into the sol state upon reaching room temperature. Moreover, injection of the precursor solution of P5L1.1/L-Arg@NU-1000 hybrid into phosphate-buffered saline (PBS) at 37 °C resulted in instantaneous formation of hydrogel (Fig. 3A), indicating that PLGA-PEG-PLGA/LAPONITE®/L-Arg@NU-1000 hybrids are suitable for use as injectable hydrogels.

The rheological properties of PLGA-PEG-PLGA/LAPONITE®/L-Arg@NU-1000 hybrids were also analyzed (Fig. 3B). The

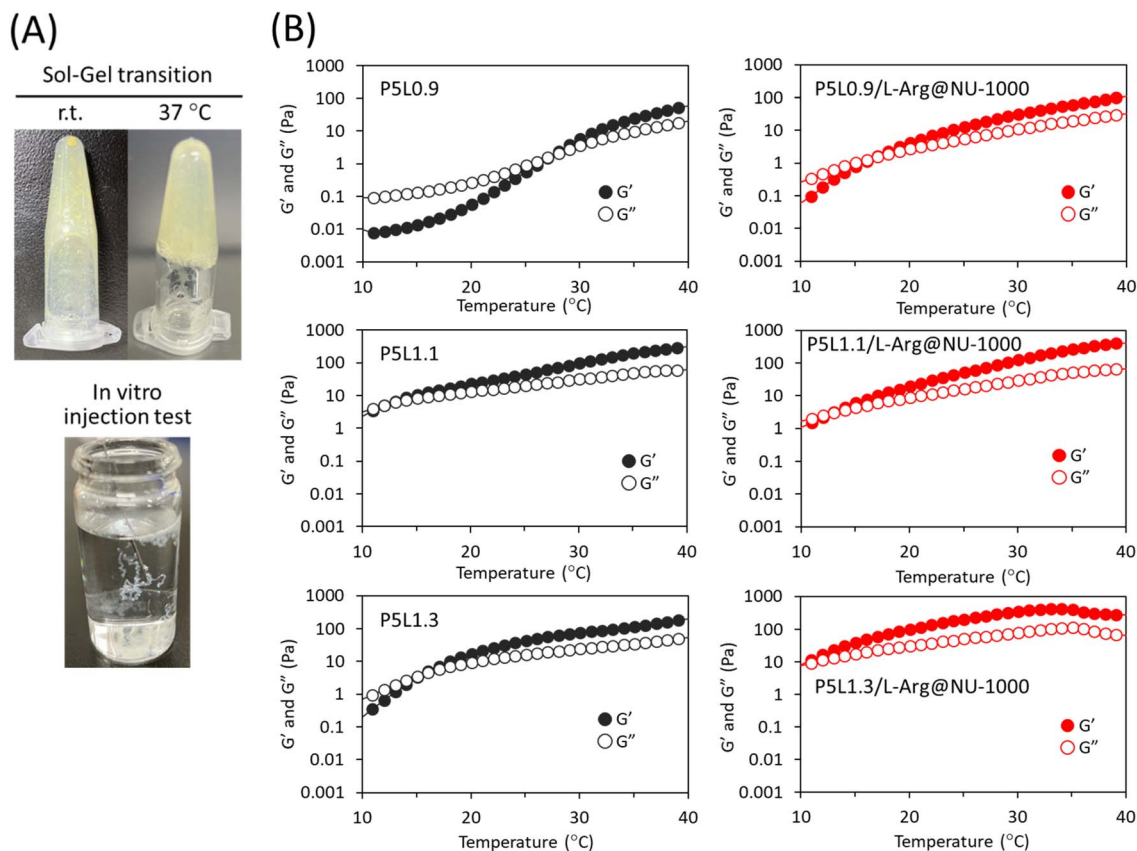


Fig. 3 (A) Representative photographs of precursor solution of P5L1.1/L-Arg@NU-1000 at room temperature and the hydrogel at 37 °C. (B) Temperature-dependent rheological properties of PLGA-PEG-PLGA/LAPONITE®/L-Arg@NU-1000 hydrogels and control PLGA-PEG-PLGA/LAPONITE® hydrogels.

Table 1 Gelation temperatures and storage moduli (G') at 37 °C of a series of PLGA-PEG-PLGA/LAPONITE®/L-Arg@NU-1000 hybrid injectable hydrogels

Samples	Gelation temp. (°C)	G' at 37 °C (Pa)
P5L0.9	28	36
P5L1.1	14	246
P5L1.3	17	55
P5L0.9/L-Arg@NU-1000	17	82
P5L1.1/L-Arg@NU-1000	13	332
P5L1.3/L-Arg@NU-1000	10	306

mechanical strength and gelation temperature of PLGA-PEG-PLGA/LAPONITE® composites were strongly affected by L-Arg@NU-1000 (Table 1). The storage moduli (G' values) of the hydrogels at 37 °C increased in the presence of L-Arg@NU-1000; the G' values of P5L0.9, P5L0.9/L-Arg@NU-1000, P5L1.1, P5L1.1/L-Arg@NU-1000, P5L1.3, and P5L1.3/L-Arg@NU-1000 at 37 °C were 36, 82, 246, 332, 55, and 306 Pa, respectively. The gelation temperature decreased in the presence of L-Arg@NU-1000, with values of 28, 17, 14, 13, 17, and 10 °C for P5L0.9, P5L0.9/L-Arg@NU-1000, P5L1.1, P5L1.1/L-Arg@NU-1000, P5L1.3, and P5L1.3/L-Arg@NU-1000, respectively. PLGA-PEG-PLGA/LAPONITE® composites prepared with higher LAPONITE®

concentrations exhibited lower gelation temperatures even in the presence of the same amount of L-Arg@NU-1000. These results indicate that the interaction between L-Arg@NU-1000 and LAPONITE® forms physical cross-linking points that facilitate formation of the hydrogel networks. As mentioned above, the capability of L-Arg@NU-1000 to alter the mechanical strength of the hybrid hydrogels *via* simple mixing is highly advantageous for increasing the mechanical compatibility of the hydrogels with tissues and organs *in vivo*. It is well known that mechanical strength of hydrogels and the network structures are strongly correlated. Therefore, to evaluate the effect of interactions between LAPONITE® and L-Arg@NU-1000 on the structure of the hydrogel networks, the P5L0.9 composite hydrogel and P5L0.9/L-Arg@NU-1000 hybrid hydrogel were analyzed using SEM (Fig. 4). The average pore size of the hydrogels decreased significantly following hybridization with L-Arg@NU-1000. The pores of the P5L0.9 hydrogel and P5L0.9/L-Arg@NU-1000 hybrid hydrogel were 454 μm^2 and 278 μm^2 , respectively, indicating that a more-dense network was formed due to hybridization with L-Arg@NU-1000. Considered collectively with the results of thermo-gelling behavior and hydrogel network structure analyses, the data suggest that L-Arg@NU-1000 interacts with LAPONITE® in the hydrogels, and the resulting binding domains form physical cross-linking points for the hydrogels that facilitate the formation of hybrid hydrogel



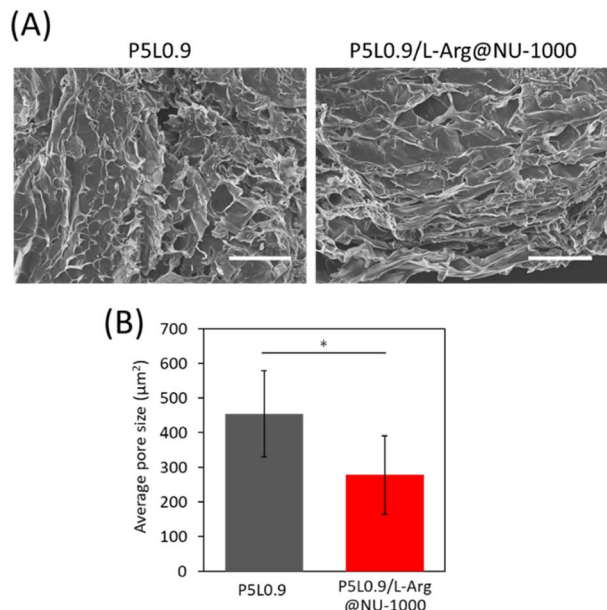


Fig. 4 (A) Representative SEM images of P5L0.9 and P5L0.9/L-Arg@NU-1000 hybrid hydrogels. (B) The average pore size of P5L0.9 and P5L0.9/L-Arg@NU-1000 hybrid hydrogels was calculated using the corresponding SEM images. * $P < 0.05$.

networks consisting of PLGA-PEG-PLGA nanomicelles, LAPONITE®, and L-Arg@NU-1000, as illustrated in (Fig. 1).

Swelling and degradation and L-arginine-release properties of hybrid hydrogels

The swelling behaviour of the hydrogels was evaluated. Hydrogels prepared with P5L0.9 and P5L0.9/L-Arg@NU-1000, incorporating varying molar ratios, exhibited pronounced swelling behavior, as illustrated in Fig. 5. Notably, hydrogel samples with lower concentrations of LAPONITE® demonstrated a markedly increased swelling ratio, which is indicative of enhanced gel stiffness resulting from denser crosslinking. This finding highlights the critical role of LAPONITE® concentration in modulating the crosslinking density and, consequently, the swelling characteristics of the hydrogels.

Biodegradation of PLGA-PEG-PLGA/LAPONITE® composite hydrogels proceeds *via* hydrolysis of PLGA-PEG-PLGA copolymers and collapse of the physical cross-linking points consisting of PLGA-PEG-PLGA nanomicelles and LAPONITE®, and this degradation of the hydrogels affects the profile of L-arginine release. Therefore, we investigated the mechanism of PLGA-PEG-PLGA/LAPONITE®/L-Arg@NU-1000 hybrid hydrogel degradation and the release of L-arginine *in vitro*. To investigate the biodegradation of PLGA-PEG-PLGA/LAPONITE®/L-Arg@NU-1000 hybrid hydrogels and control PLGA-PEG-PLGA/LAPONITE® composite hydrogels, PBS was added on top of the hydrogels, and the hydrogels were incubated at 37 °C. At 5, 10, 15, and 21 days, the supernatant was completely removed, and the hydrogels were dried by lyophilization and then weighed. (Fig. 5) Shows the change in hydrogel dry weight over time during the degradation test. All of the hydrogels degraded

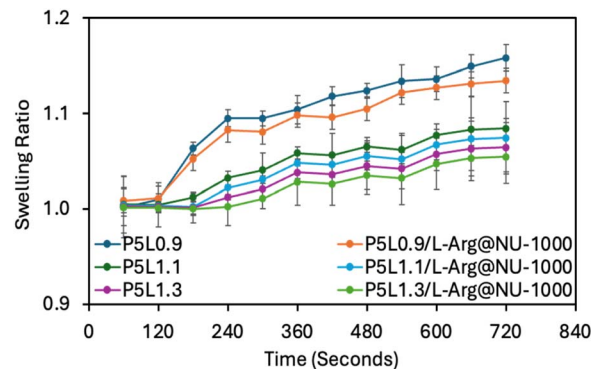


Fig. 5 Swelling ratio quantification from the hybrid hydrogels at time (0 to 680) seconds. Data are expressed as mean \pm SD.

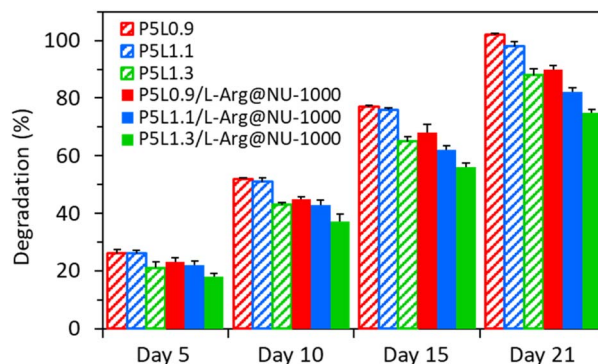


Fig. 6 Cumulative degradation profiles of PLGA-PEG-PLGA/LAPONITE®/L-Arg@NU-1000 hybrid hydrogels and control PLGA-PEG-PLGA/LAPONITE® hydrogels.

gradually. The degradation rate of the control PLGA-PEG-PLGA/LAPONITE® composite hydrogels decreased with increasing LAPONITE® concentrations. The degradation rate of the PLGA-PEG-PLGA/LAPONITE®/L-Arg@NU-1000 hybrid hydrogels also decreased with increasing LAPONITE® concentrations. Interestingly, the PLGA-PEG-PLGA/LAPONITE®/L-Arg@NU-1000 hybrid hydrogels degraded at a significantly slower rate than the corresponding control PLGA-PEG-PLGA/LAPONITE® composite hydrogels. As mentioned above, L-Arg@NU-1000 forms physical cross-linking points in the hybrid hydrogels *via* hydrogen bonds with LAPONITE®, thereby facilitating the formation of a dense hydrogel network that may slow the rate of collapse of the physical cross-linking points.

We then investigated the release of L-arginine from the hybrid hydrogels. PBS was added on top of the hydrogels, and the hydrogels were incubated at 37 °C for a predetermined time, after which the supernatant was analysed using a ninhydrin assay to quantify the amount of L-arginine released from the hydrogels. As shown in (Fig. 2B), although all of the L-arginine loaded to NU-1000 was released after only 7 days, the rate of L-arginine release from the PLGA-PEG-PLGA/LAPONITE®/L-Arg@NU-1000 hybrid hydrogels was significantly lower than that for NU-1000 alone, and the hybrid hydrogels exhibited sustained slow release of L-arginine over a 1-month period



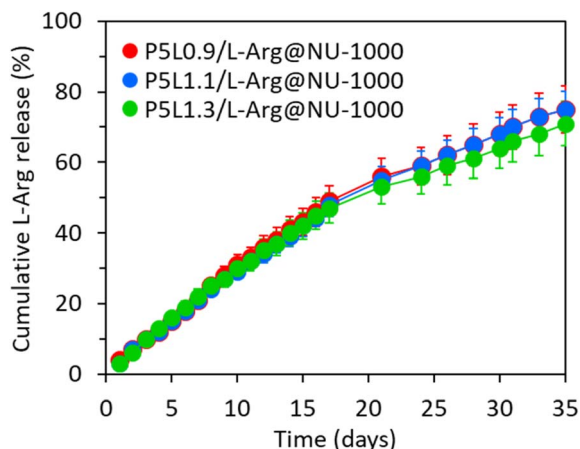


Fig. 7 Profile of cumulative L-arginine release from PLGA-PEG-PLGA/LAPONITE@L-Arg@NU-1000 hybrid hydrogels.

without a burst release (Fig. 7). A comparison of the properties of L-arginine release indicated that hybrid hydrogels prepared with higher LAPONITE® concentrations exhibited a lower release rate. This result agreed well with the results of biodegradation rate analyses (Fig. 6), suggesting that biodegradation of the hybrid hydrogels is a crucial step in the release of L-arginine. These results also suggest that L-arginine released from NU-1000 within the hybrid hydrogels adsorbs onto LAPONITE® *via* hydrogen bonding between the carboxyl and amino groups of L-arginine and the hydroxyl groups of LAPONITE®, which slows the release of L-arginine from the

hybrid hydrogels. Consequently, the three-dimensional network structure of hybrid hydrogels containing LAPONITE® functions as a secondary carrier for L-arginine to achieve sustained slow release. Importantly, due to the sustained slow release of L-arginine by the hybrid hydrogels, the concentration of L-arginine within the hybrid hydrogels remains sufficiently high for a long period of time. This suggests that L-arginine exerts angiogenic effects both within the hybrid hydrogels and externally.

Cytocompatibility of the hybrid hydrogels

The cytocompatibility of each component of the PLGA-PEG-PLGA/LAPONITE®/L-Arg@NU-1000 hybrid hydrogel (P5L1.1/L-Arg@NU-1000) was examined using an *in vitro* live/dead assay with human umbilical vein endothelial cells (HUVECs). P5L1.1/NU-1000 hydrogels (without L-arginine) exhibited high cytocompatibility after 1 day (97% cell survival), and the cell viability was almost the same as that of P5L1.1 hydrogels (100%), indicating that NU-1000 is cytocompatible. P5L1.1/L-Arg hydrogels (without NU-1000) also exhibited high cytocompatibility after 1 day (96% cell survival), and the cell viability was almost the same as that of P5L1.1 hydrogels (100%), indicating that hydrogels containing L-arginine at the specific concentration used in this study are cytocompatible. As expected from these results, HUVECs cultured with P5L1.1/L-Arg@NU-1000 hybrid hydrogels for 1 day exhibited a well-spread morphology and 100% viability (Fig. 8A), indicating the hybrid hydrogels are not cytotoxic. We then examined the proliferation of HUVECs cultured with hybrid hydrogels for 7 days. HUVECs cultured

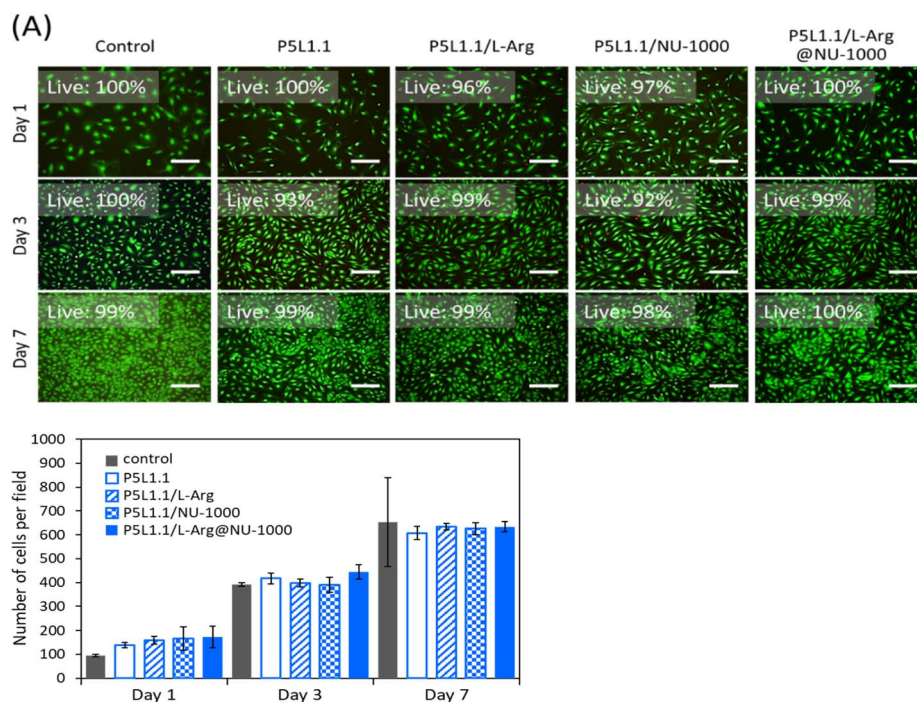


Fig. 8 (A) Representative fluorescence microscopy images of HUVECs cultured for 1, 3, and 7 days with P5L1.1/L-Arg@NU-1000 hybrid hydrogels and control hydrogels and examined using live/dead cell assays. Scale bars indicate 100 μ m. (B) Number of HUVECs detected in the fields of the corresponding microscopy images.



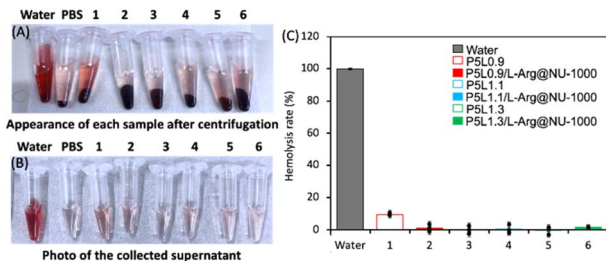


Fig. 9 Haemolytic activity of the injectable hydrogels. (A) Representative digital images of each sample after 1-hour incubation followed by centrifugation. (B) Visual appearance of the supernatants collected post-centrifugation. (C) Quantitative analysis of hemolysis rate after 1 hour exposure, with comparison to Milli-Q water as the positive control. Data are expressed as mean \pm SD.

with P5L1.1/L-Arg@NU-1000 hybrid hydrogels exhibited good proliferation, and the proliferation rate was almost the same as that of control cells (Fig. 8B).

Next we evaluated compatibility of the hybrid hydrogels against Red blood cells. As shown in Fig. 9A and B, no hemolytic

activity was observed in the gel itself and in its degradation products. These results indicate that the hybrid hydrogel components as a whole, as well as their degradation products, are nontoxic to surrounding HUVECs and red blood cells. Based on these results, we proceeded to *in vivo* experiments to assess the angiogenic efficacy of the hybrid hydrogels.

In vivo angiogenic capabilities of hybrid hydrogels

Considering the abovementioned evidence indicating that PLGA-PEG-PLGA/LAPONITE@/L-Arg@NU-1000 hybrid hydrogels promote angiogenesis, the hybrid hydrogels were subjected to *in vivo* angiogenesis assays. We first evaluated neo-vascularization in hybrid hydrogels and control hydrogels without L-arginine and/or NU-1000. As the PLGA-PEG-PLGA/LAPONITE@/L-Arg@NU-1000 hybrid hydrogels are injectable, precursor solutions of the hybrid hydrogels were administered by injection into the subcutaneous tissue of mice, and hydrogel promotion of angiogenesis in the surrounding tissues was quantified at 7, 14, and 21 days. Representative images of the hydrogels and surrounding tissues are shown in (Fig. S4 and S6, SI), and angiogenesis scores are shown in (Fig. 10). At 21 days,

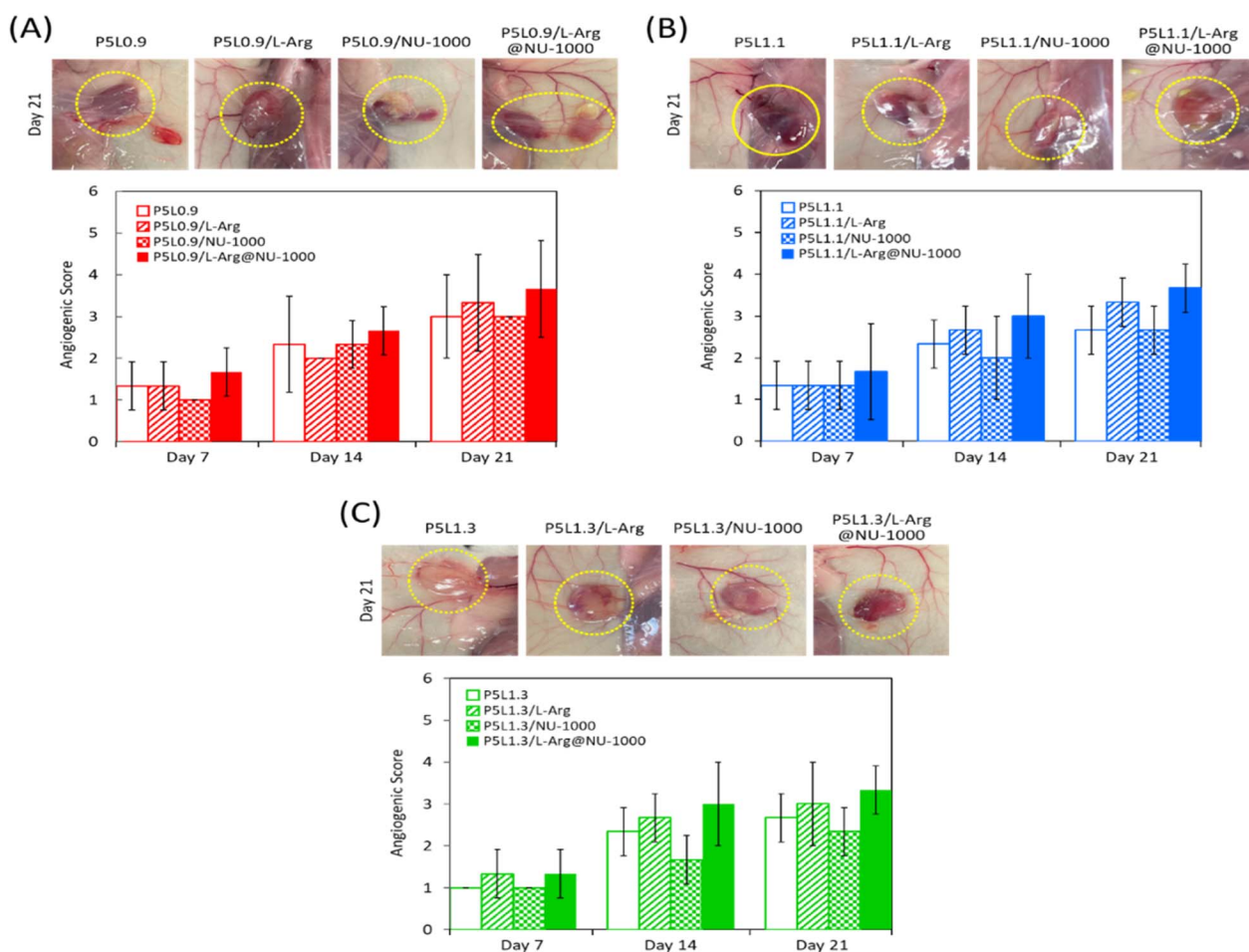


Fig. 10 Representative images and angiogenesis scores of hydrogels surrounded by tissues at day 21 after administration of PLGA-PEG-PLGA/LAPONITE@/L-Arg@NU-1000 hybrid hydrogels and control hydrogels for (A) P5L0.9 series, (B) P5L1.9 series, and (C) P5L1.3 series. Yellow dotted circles indicate hydrogels formed *in vivo*.



P5L0.9/NU-1000 hydrogels (without L-arginine) exhibited the same angiogenesis score (3.0) as P5L0.9 hydrogels, indicating that NU-1000 alone does not suppress the angiogenic capability of the hydrogels at the concentrations used in this study. P5L0.9/L-Arg hydrogels (without NU-1000) exhibited a slightly higher angiogenesis score (3.3) than P5L0.9 hydrogels (3.0) at 21 days, indicating that L-arginine released from the hydrogels promoted angiogenesis due to the inherent bioactivity. Notably, P5L0.9/L-Arg@NU-1000 hybrid hydrogels exhibited a higher angiogenesis score (3.7) than P5L0.9/L-Arg hydrogels (3.3) at 21 days. Moreover, a number of blood vessels penetrating the P5L0.9/L-Arg@NU-1000 hybrid hydrogels were detected, and the hydrogels exhibited a deep red color indicative of the formation of a large number of blood vessels. A similar tendency was observed for a series of P5L1.1- and P5L1.3-based hybrid hydrogels. Importantly, newly formed blood vessels in the

hydrogels were composed of host vein endothelial cells, indicating that L-arginine released from the hydrogels acted upon the surrounding vein endothelial cells in the subcutaneous tissue of the host. Thus, these results demonstrate that the sustained slow release of L-arginine by the hybrid hydrogels is due to the functionality of NU-1000 as a primary carrier, which efficiently facilitates angiogenesis *in vivo*.

To evaluate the angiogenic capability of the hybrid hydrogels in greater detail, we prepared section samples of hydrogels implanted in mice for 21 days and then visualized newly formed blood vessels in the hydrogels using immunofluorescence staining of CD31. Representative images are shown in (Fig. S7 and S9, SI), and the number of newly formed blood vessels in the hydrogels and their average diameter are illustrated in (Fig. 11). CD31-positive cells were observed over the entire examined area, and they were also detected around luminal

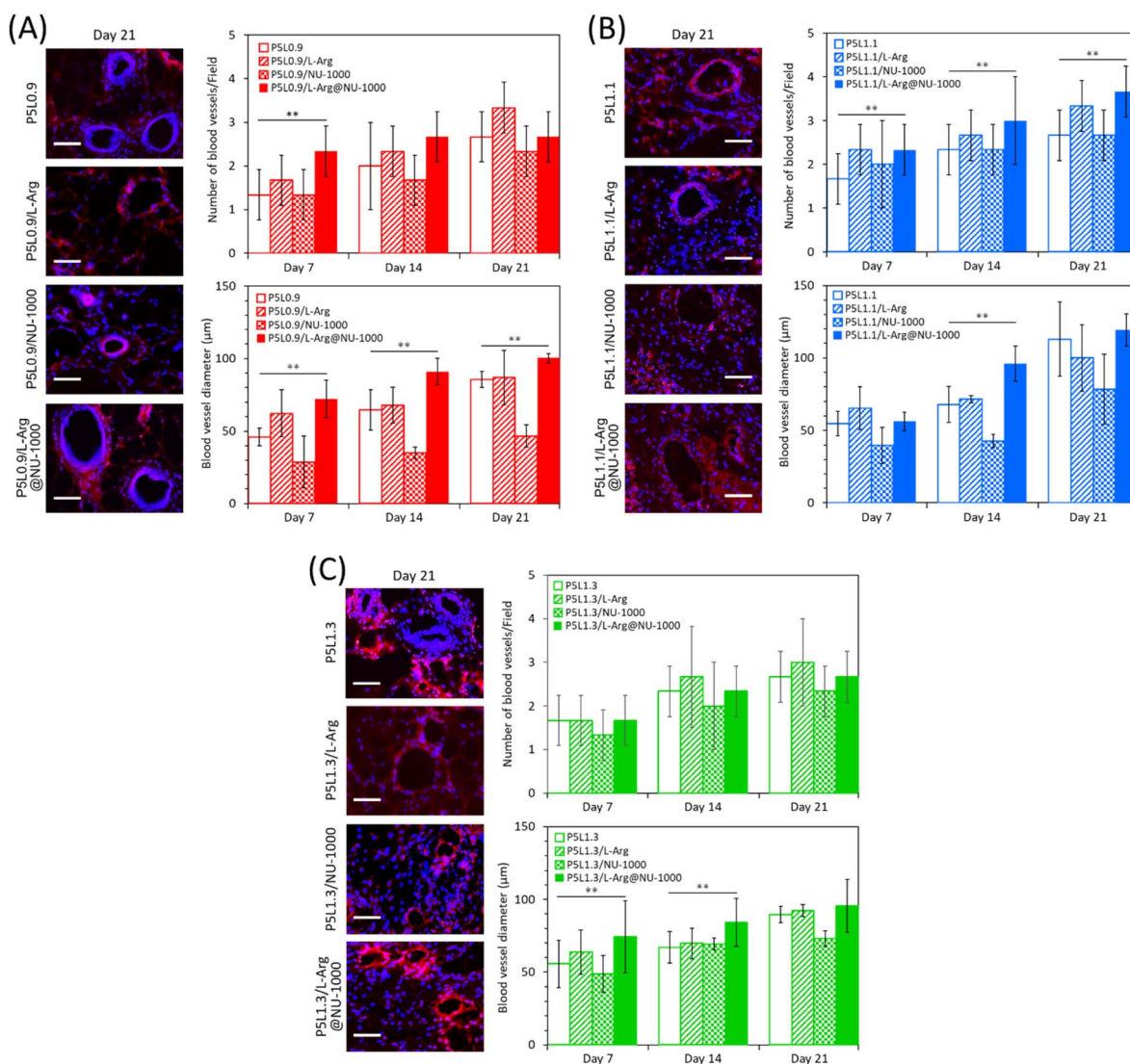


Fig. 11 Representative fluorescence microscopy images of newly formed blood vessels in hydrogels *in vivo* subjected to immunofluorescence staining of CD31 and the number and diameter of blood vessels at days 7, 14, and 21 after administration of PLGA-PEG-PLGA/LAPONITE®/L-Arg@NU-1000 hybrid hydrogels and control hydrogels for (A) P5L1.1 series, (B) P5L1.1 series, (C) P5L1.3 series. Scale bars indicate 100 μm. Blue: DAPI; red: CD31 (Alexa Fluor® 567).



structures, indicating blood vessel formation in the hydrogels. At 21 days, P5L1.1/NU-1000 hydrogels (without L-arginine) exhibited a similar number of blood vessels as P5L1.1 hydrogels, but the average diameter of blood vessels in P5L1.1/NU-1000 hydrogels was markedly smaller than that of blood vessels in the P5L1.1 hydrogels. P5L1.1/L-Arg hydrogels (without NU-1000) exhibited a higher number of blood vessels than P5L1.1 hydrogels at 21 days, but the average diameter of blood vessels in the P5L1.1/L-Arg hydrogels was smaller than that of blood vessels in P5L1.1 hydrogels. By contrast, the P5L1.1/L-Arg@NU-1000 hybrid hydrogels exhibited both a higher number of blood vessels and larger average diameter at 21 days than did P5L1.1/L-Arg hydrogels. These results indicate that L-arginine is sustainably released from NU-1000 and subsequently promotes blood vessel formation by host vein endothelial cells. A similar tendency was observed for a series of P5L1.1- and P5L1.3-based hybrid hydrogels. Accordingly, these results demonstrate that PLGA-PEG-PLGA/LAPONITE®/L-Arg@NU-1000 hybrid hydrogels function not only as carriers of L-arginine but also as scaffolds for host vein endothelial cells, thereby accelerating vascularization *in vivo*. The capability of our hybrid injectable hydrogels to stably load L-arginine-adsorbing NU-1000 and deliver that cargo to desired locations in the body represents a distinct advantage compared with current hydrogel-based scaffolds composed of polymers only (*i.e.*, that do not utilize MOFs). Considered collectively, our data confirm that PLGA-PEG-PLGA/LAPONITE®/L-Arg/NU-1000 hybrid injectable hydrogels provide a superior microenvironment for angiogenesis and demonstrate the potential utility of these hydrogels for *in vivo* tissue engineering applications.

Conclusions

Herein, we proposed a novel, hybrid-type injectable hydrogel generated by hybridizing MOFs NU-1000 with biodegradable PLGA-PEG-PLGA/LAPONITE® composites. Large amounts of L-arginine can be loaded to NU-1000 interior pores, such that hybridized PLGA-PEG-PLGA/LAPONITE®/L-Arg@NU-1000 hydrogels exhibit sustained slow release of L-arginine over a 1-month period. The precursor aqueous solution of PLGA-PEG-PLGA/LAPONITE®/L-Arg@NU-1000 undergoes rapid sol-gel transition upon exposure to body temperature, enabling focal administration of the hydrogels at desired locations in the body *via* simple injection. The sustained slow release of L-arginine by the hybrid hydrogels due to the functionality of NU-1000 as a primary carrier efficiently promotes angiogenesis *in vivo*. The results of this study not only demonstrated the utility of NU-1000 as a nanocarrier for L-arginine to accelerate angiogenesis *in vivo* but also the availability of L-arginine-loaded NU-1000 as a novel component in the design of scaffolding materials for *in vivo* tissue engineering, as neovascularization is an essential process in the regeneration and functional recovery of injured tissues. The resultant hybrid hydrogels exhibit specific functions that cannot be achieved using NU-1000 or PLGA-PEG-PLGA/LAPONITE® hydrogels alone. Thus, the hybrid injectable hydrogels have the potential to become a new type of scaffolding material for *in vivo* tissue engineering applications

targeting a wide range of tissues and organs. To the best of our knowledge, this is the first reported example of nanoscale MOF-injectable hydrogel hybrid scaffolds.

Author contributions

S. S.: experimentation of the nanocomposite hydrogels, investigations, analysis, methodology, data curation, writing. D. T.: conducted most of the animal experiments, investigation, methodology. S. K.: analysis hemolytic activity experiment. F. M.: preparation and analysis of NU1000. T. T.: conducted MOF-related experiments, methodology, review, and editing. N. K.: conceptualization, project administration, writing – review and editing, funding acquisition.

Conflicts of interest

There are no conflicts to declare.

Data availability

A data are available upon reasonable request.

Supplementary information: characterization and structure of the synthesized polymers and Nu-1000, images of the gels *in vivo*, microscopic images of the immune-stained gels. See DOI: <https://doi.org/10.1039/d5ra02770e>.

Acknowledgements

This research was supported by JSPS KAKENHI (Grant Number 22K19925).

References

- 1 H. Li, M. Eddaoudi, M. O'Keeffe and O. M. Yaghi, *Nature*, 1999, **402**, 276–279.
- 2 Y. He, W. Zhou, G. Qian and B. Chen, *Chem. Soc. Rev.*, 2014, **43**, 5657–5678.
- 3 S. Kitagawa, *Acc. Chem. Res.*, 2017, **50**, 514–516.
- 4 H. Daglar, H. C. Gulbalkan, G. Avci, G. O. Aksu, O. F. Altundal, C. Altintas, I. Erucar and S. Keskin, *Angew Chem. Int. Ed. Engl.*, 2021, **60**, 7828–7837.
- 5 S. Denning, A. A. A. Majid, J. M. Lucero, J. M. Crawford, M. A. Carreon and C. A. Koh, *ACS Appl. Mater. Interfaces*, 2020, **12**, 53510–53518.
- 6 Y. Shen, T. Pan, L. Wang, Z. Ren, W. Zhang and F. Huo, *Adv. Mater.*, 2021, **33**, 2007442.
- 7 M. Li, J. Chen, W. Wu, Y. Fang and S. Dong, *J. Am. Chem. Soc.*, 2020, **142**(36), 15569–15574.
- 8 E. A. Dolgoplova, A. M. Rice, C. R. Martin and N. B. Shustova, *Chem. Soc. Rev.*, 2018, **47**, 4710–4728.
- 9 L. E. Kreno, K. Leong, O. K. Farha, M. Allendorf, R. P. Van Duyne and J. T. Hupp, *Chem. Rev.*, 2012, **112**, 1105–1125.
- 10 P. Horcajada, T. Chalati, C. Serre, B. Gillet, C. Sebrie, T. Baati, J. F. Eubank, D. Heurtaux, P. Clayette, C. Kreuz, J.-S. Chang, Y. K. Hwang, V. Marsaud, P.-N. Bories,

- L. Cynober, S. Gil, G. Ferey, P. Couvreur and R. Gref, *Nat. Mater.*, 2010, **9**, 172–178.
- 11 X. Zhao, S. He, B. Li, B. Liu, Y. Shi, W. Cong, F. Gao, J. Li, F. Wang, K. Liu, C. Sheng, J. Su and H.-G. Hu, *Nano Lett.*, 2023, **23**, 863–871.
- 12 S. Mallakpour, E. Nikkhoo and C. M. Hussain, *Coord. Chem. Rev.*, 2022, **451**, 214262.
- 13 X. Yao, X. Chen, Y. Sun, P. Yang, X. Gu and X. Dai, *Regener. Biomater.*, 2024, **11**, rbae009.
- 14 J. Wu, S. Jiang, W. Xie, Y. Xue, M. Qiao, X. Yang, X. Zhang, Q. Wan, J. Wang, J. Chen and X. Pei, *J. Mater. Chem. B*, 2022, **10**, 8535–8548.
- 15 T. Katayama, S. Tanaka, T. Tsuruoka and K. Nagahama, *ACS Appl. Mater. Interfaces*, 2022, **14**, 34443–34454.
- 16 K. Huang, W. Liu, W. Wei, Y. Zhao, P. Zhuang, X. Wang, Y. Wang, Y. Hu and H. Dai, *ACS Nano*, 2022, **16**, 19491–19508.
- 17 M. Shyngys, J. Ren, X. Liang, J. Miao, A. Blocki and S. Beyer, *Front. Bioeng. Biotechnol.*, 2021, **9**, 603608.
- 18 X. Li, X. Shu, Y. Shi, H. Li and X. Pei, *Chin. Chem. Lett.*, 2023, **34**, 107986.
- 19 J. Lin, C. Zong, B. Chen, T. Wang, J. Xu, J. Du, Y. Lin, Y. Gu and J. Zhu, *RSC Adv.*, 2023, **13**, 5600–5608.
- 20 L. Zhong, J. Chen, Z. Ma, H. Feng, S. Chen, H. Cai, Y. Xue, X. Pei, J. Wang and Q. Wan, *Nanoscale*, 2020, **12**, 24437–24449.
- 21 Y. Zeng, C. Wang, K. Lei, C. Xiao, X. Jiang, W. Zhang, L. Wu, J. Huang and W. Li, *Adv. Healthcare Mater.*, 2023, **19**, e2300250.
- 22 Y. Yu, G. Chen, J. Guo, Y. Liu, J. Ren, T. Kong and Y. Zhao, *Mater. Horiz.*, 2018, **5**, 1137–1142.
- 23 A. Abednejad, A. Ghaee, J. Nourmohammadi and A. A. Mehrizi, *Carbohydr. Polym.*, 2019, **222**, 115033.
- 24 M. Zhang, G. Wang, X. Zhang, Y. Zheng, S. Lee, D. Wang and Y. Yang, *Polymers*, 2021, **13**, 3151.
- 25 Y. Jiang, X. Pan, M. Yao, L. Han, X. Zhang, Z. Jia, J. Weng, W. Chen, L. Fang, X. Wang, Y. Zhang, R. Duan, F. Ren, K. Wang, X. Chen and X. Lu, *Nano Today*, 2021, **39**, 101182.
- 26 M. Yin, J. Wu, M. Deng, P. Wang, G. Ji, M. Wang, C. Zhou, N. T. Blum, W. Zhang, H. Shi, N. Jia, X. Wang and P. Huang, *ACS Nano*, 2021, **15**, 17842–17853.
- 27 H. Wang, H. Wan, Q. Wang, Y. Ma, G. Su, X. Cao and H. Gao, *Smart Mater. Med.*, 2023, **4**, 480–492.
- 28 M. Rezaeeyazdi, T. Colombani, A. Memic and S. A. Bencherif, *Materials*, 2018, **11**, 1374.
- 29 Z. Y. Luo, J. J. Pan, Y. H. Sun, S. Q. Zhang, Y. Yang, H. Liu, Y. Li, X. Xu, Y. Sui and S. C. Wei, *Adv. Funct. Mater.*, 2018, **28**, 1804335.
- 30 J. E. Mealy, J. J. Chung, H.-H. Jeong, D. Issadore, D. Lee, P. Atluri and J. A. Burdick, *Adv. Mater.*, 2018, **30**, 1705912.
- 31 K. Ono, H. Hashimoto, T. Katayama, N. Ueda and K. Nagahama, *Biomacromolecules*, 2021, **22**, 4217–4227.
- 32 K. Nagahama, N. Oyama, K. Ono, A. Hotta, K. Kawauchi and T. Nishikata, *Biomater. Sci.*, 2018, **6**, 550–561.
- 33 M. Miyazaki, T. Maeda, K. Hirashima, N. Kurokawa, K. Nagahama and A. Hotta, *Polymer*, 2017, **115**, 246–254.
- 34 J. E. Mondloch, W. Bury, D. Fairen-Jimenez, S. Kwon, E. J. Demarco, M. H. Weston, A. A. Sarjeant, S. T. Nguyen, P. C. Stair, R. Q. Snurr, O. K. Farha and J. T. Hupp, *J. Am. Chem. Soc.*, 2013, **135**, 10294–10297.
- 35 S. Ahn, S. L. Nauert, C. T. Buru, M. Rimoldi, H. Choi, N. M. Schweitzer, J. T. Hupp, O. K. Farha and J. M. Notestein, *J. Am. Chem. Soc.*, 2018, **140**, 8535–8543.
- 36 M. Ghadiri, W. Chrzanowski, W. H. Leeb and R. Rohani Zadeh, *RSC Adv.*, 2014, **4**, 35332.
- 37 I.-S. Park, S.-W. Kang, Y.-J. Shin, K.-Y. Chae, M.-O. Park, M.-Y. Kim, D. N. Wheatley and B.-H. Min, *Br. J. Cancer*, 2003, **89**, 907–914.
- 38 N. Kazemi, M. J. Mahalati, Y. Kaviani, M. H. Al-Musawi, J. Varshosaz, S. S. E. Bakhtiari, M. Tavakoli, M. Alizadeh, F. Sharifianjazi, S. Salehi, A. Najafinezhad and M. Mirhaj, *Int. J. Pharm.*, 2024, **653**, 123931.
- 39 S. S. Islam, T. Dode, S. Kawashima, M. Fukuoka, T. Tsuruoka and K. Nagahama, *Gels*, 2025, **11**, 514.
- 40 C. A. Staton, S. M. Stribbling, S. Tazzyman, R. Hughes, N. J. Brown and C. E. Lewis, *Int. J. Exp. Pathol.*, 2004, **85**, 233–248.
- 41 N. Oyama, H. Minami, D. Kawano, M. Miyazaki, T. Maeda, T. K. oma, A. Hotta and K. Nagahama, *Biomater. Sci.*, 2014, **2**, 1057–1062.

